9132 J. Phys. Chem. A **2002,** *106,* 9132−9144

Electron Localization in Solid Acetonitrile

Ilya A. Shkrob,*,† Keiji Takeda,‡,§ and Ffrancon Williams‡

Chemistry Division, Argonne National Laboratory, Argonne, Illinois 60439 and
Department of Chemistry, University of Tennessee, Knoxville, Tennessee 37996-1600

Received: March 20, 2002; In Final Form: June 17, 2002

Electron localization in the bulk condensed phases of acetonitrile differs drastically from the corresponding processes that take place in water and aliphatic alcohols. In particular, electron capture following the ionization of liquid and solid acetonitrile yields well-defined radical anions in place of the largely structureless solvated and trapped electrons characteristic of irradiated solutions and rigid glasses. This is remarkable given the many similarities that exist not only between the intrinsic properties of these individual solvent molecules, such as polarity, but also in their cooperative capacity to function as solvents. Here, with the aid of detailed experimental and computational studies, we examine on a fundamental level what gives rise to such a sharp contrast in the behavior of these alkyl cyanides as compared to water and alcohols. EPR and optical spectra, and *ab initio* calculations on the radical anions are used together with diffraction data for the crystal structures to demonstrate that electron attachment to nitrile molecules in the crystalline state results in a significant bending of the linear CCN moiety. Moreover, in the formation of the dimer anions, which only takes place in certain crystalline phases, it is determined that the intermolecular bonding occurs between the cyanide carbons in an antiparallel arrangement. A staggered structure for the dimer anion in α-acetonitrile is then suggested, in which there is a nearly coplanar arrangement with the two bent CCN fragments. The resulting structure accounts for the observed EPR parameters, the position of the UV−vis absorption band, and the trends observed in the vibronic progressions for the four H/D isotopomers. The dimer radical anion in α-acetonitrile retains the same orientation and symmetry as that of the preexisting neutral $\{CH_3CN\}_2$ pairs in this crystal despite the resulting changes in molecular geometry and in the translational coordinates for the cyanide carbons as the two acetonitrile molecules come together. We suggest that dimer anions of nitriles can form only in the phases where such “antiparallel” pairs occur, including liquid systems; otherwise, the electron remains attached to a single molecule, as in β-acetonitrile. Because electron capture by water or alcohol molecules in the condensed phase appears to require larger molecular clusters, the contrast between the behavior of these solvents and acetonitrile is attributable to the relative ease with which acetonitrile molecules in the crystal or solvent can undergo valence-electron attachment via their accessible low-lying π^* orbitals.

1. Introduction

Irradiation of organic solids with high-energy particles at low temperatures yields neutral radicals and trapped charges. In some solids, such as alcohol and alkane glasses whose individual molecules lack a positive electron affinity, the negatively charged entities that are produced by the irradiation are generally referred to as “trapped electrons” or “polarons”, reminiscent of the well-known *F*-centers which are similarly generated in the crystalline alkali halides.[1−7] These species are commonly described by a lattice-type model in which the “trapped electron” is viewed as a single quantum-mechanical particle residing in a potential well.[2−7] In aqueous and organic glasses, the “trap” in its simplest form is regarded as a spherical cavity surrounded by solvent molecules that are polarized by the excess negative charge residing at its center. This picture implies that the excess electron and the solvent electrons are separable. Although this approximation is poorly justified,[2] the model has been used to explain the variation in some of the spectral properties (broad optical absorption bands and magnetic resonance line widths) of these “trapped electrons” with solvent polarity.

Despite the common assumption that the excess electron in trapped or solvated electrons is localized on a solvent molecule or on a small group of solvent molecules, there is in fact scant physical evidence for the formation of well-defined radical anions in many molecular solids and liquids exposed to high-energy radiation.[1,2] For this reason, the very few cases of organic solids for which the mode of electron localization is known, mainly through studies by Electron Paramagnetic Resonance (EPR) spectroscopy, deserve particular attention. Alkyl cyanides provide examples of such solids, and acetonitrile, CH_3CN, is a particularly interesting case since many of its gas-phase and solution properties are similar to those of water and alcohols. These properties will now be reviewed briefly before taking up the subject of solid acetonitrile.

In the gas phase, the CH_3CN monomer molecule has a large dipole moment of 4.3 D, an adiabatic electron affinity of 17 meV, and a negative vertical electron affinity of −2.84 eV.[8] CH_3CN^- is a dipole-bound anion with the electron in a diffuse orbital (>3 nm).[8a,9,10] Although the C_{2h} symmetric $\{CH_3CN\}_2$

---

* To whom correspondence should be addressed.

† Chemistry Division, Argonne National Laboratory.

‡ Department of Chemistry, University of Tennessee.

§ Present address: T-403, Chuuou 3-7, Sayamashi, Saitama, Japan 350-1308.

10.1021/jp020759s CCC: $22.00

TABLE 1: EPR Parameters for $(CD_3CN)_2^-$ Anion (Site-1) in γ-Irradiated Monoclinic α-Acetonitrile-d_3 at 77 K

nucleus	hfcc, isotropic	component	hfcc	hfcc, dipole	x^d	y^d	$z\|\|\mathbf{a}^d$
^{14}N	+7.0	**aa**	0.0 *(0 ± 3)*[a]	−7.0			
		bb	3.5 *(0 ± 3)*[a]	−3.5			
		cc	17.5	10.5	0.785	−0.45	−0.425
^{13}CD$_3$	+19.73 *(19.6)*[a]	**aa**	17.4	−2.3	0.611	−0.676	0.412
		bb	18.8 *(18.7)*[a]	−0.9	0.053	0.555	0.830
		cc	23 *(22.8)*[a]	3.3	0.789	0.485	−0.375
^{13}CN[a]	−1.5	**aa**	−8	−6.5	*b*		
		bb	0	1.5			
		cc	5	6.5	*c*		
g-tensor		**aa**	2.0010		−0.339	−0.917	0.212
		bb	2.0042		0.544	−0.007	0.839
		cc	2.0023		0.768	−0.400	−0.501

Hyperfine coupling constants (hfcc) are given in Gauss ($1G = 10^{-4}$ T); the principal values of the hfc tensors (column 3) are separated into the isotropic (Fermi) and dipolar contributions (columns 2 and 4, respectively). See Figure 2S for stereographic projection of the tensor axes on the *xy* plane. The data are given for the site-1 variant of ^{13}CD$_3$CN (see Table 1S for g- and hfc tensors and directional cosines for all three isotopomers and both sites). [a] From refs 19 and 30; there is uncertainty about the relative signs for the hfc constants for ^{13}CN, which are (±5, ±8, 0). The signs given above are suggested by our DFT calculations; also, one would expect a small angle between the long axes of the hfc tensors (i.e., 2*p* orbitals) for ^{14}N and ^{13}CN. [b] Within 13° of the **b** axis of the g tensor. [c] Within 16° of the **c** axes of the g and ^{14}N tensors. [d] Directional cosines of the principal axes; axis *z* is collinear with the crystallographic axis **a**; axes *x* and *y* are normal to **a**.

dimer readily forms in the vapor (the heat of dimerization is estimated to be −0.21[11] or −0.23 eV,[12] which is close to the energy of the hydrogen bond for alcohols), the dimer anion, $\{CH_3CN\}_2^-$, has never been observed. In the trimer $\{CH_3CN\}_3$, one of the monomers couples sideways to the C_{2h} pair,[8a,12] such that this monomer molecule binds the electron in the same way as the CH$_3$CN monomer; the adiabatic electron affinity of the trimer (14−20 meV) is higher than that of the monomer.[8a] Higher multimer anions, $\{CH_3CN\}_n^-$, were found only for $n > 12$; these anions were prepared by collisional electron transfer from high-Rydberg Kr** atoms.[13] Thus, many molecules are needed to stabilize the negative charge, very similar to the situation found for gas-phase clusters of alcohols and water.[14] It would therefore be reasonable to expect that acetonitrile solvates and traps electrons in much the same way as these protic solvents. However, this is not the case, as described below.

In liquid acetonitrile (−30 to 50 °C), two reducing species are present in the first 1−3 μs after the ionization:[15] these consist of the high-temperature form, anion-1, that absorbs in the 1−2 μm region, and the low-temperature form, anion-2, that absorbs in the 400−800 nm region.[15−18] Anion-2 is ≈0.46 eV more stable than anion-1.[15,18] These two anions are in dynamic equilibrium, the interconversion occurring in 3 ns at 25 °C,[18] and in 20−50 ns at −30 °C.[15] It has been shown[18] (i) that anion-1 is a high-mobility species whose room-temperature diffusion coefficient is >3.3 times higher than that of other ions, including anion-2, (ii) the activation energy for this rapid migration is ∼3.2 kJ/mol while that of other ions (including anion-2) is 7.4 to 7.6 kJ/mol, (iii) electron-transfer reactions that involve anion-1 proceed with rate constants $\sim 10^{11}$ M^{-1} s^{-1}, which is 10 times the rate constant for other species, and (iv) photoexcitation of anion-1 and anion-2 in their respective bands causes their fragmentation to CH$_3$ and CN$^-$. Originally,[15,17,19] it has been suggested that anion-1 and anion-2 are the monomer and the dimer radical anions of acetonitrile, respectively. On the other hand, the recent study of Shkrob and Sauer[18] suggests that the IR-absorbing anion-1 is likely to be a multimer anion related to the "solvated/trapped electron" in saturated hydrocarbons (see ref 18 for more detail). However, neither pulse radiolysis nor photoconductivity can provide much direct insight into the electronic structure of these two species.

Such insights are provided by EPR and optical studies carried out in the 1960s and 1970s on the radical anions produced by irradiation of crystalline alkyl cyanides.[19−30] The main results of these studies are summarized in the 1982 review by Williams and Sprague.[19] Irradiated single crystal and polycrystalline samples of frozen alkyl cyanides were found to yield either monomer or dimer radical anions with distinct EPR signatures. In practice, most of the EPR results were obtained with deuterated compounds because the radical anion spectra in the protiated nitriles were often obscured by proton hyperfine broadening as well as overlapping signals from the concomitant formation of neutral radicals such as $^\bullet$CH$_2$CN. Nevertheless, it has been established from both optical[19] and EPR studies[28] that essentially the same radical anion species are formed in the H/D isotopomers of acetonitrile. For example, EPR studies on the dimer radical anion in α-acetonitrile have verified that the ^{14}N hyperfine tensor of the perprotio anion in acetonitrile-h$_3$ is exactly the same as that determined for the perdeuterio anion in acetonitrile-d_3.[28]

Significantly, the particular radical anion that is formed in a given solid nitrile depends critically on the crystal structure. This is well illustrated by acetonitrile, for which there are two distinct crystalline phases, namely monoclinic α-acetonitrile (stable between 217 and 229 K)[31] and orthorhombic β-acetonitrile (stable below 217 K).[32] Because the upper phase is invariably obtained by quenching the sample from above the transition temperature, it is possible therefore to study either phase at the much lower temperatures where the radical anions are metastable. Upon γ-irradiation, α-acetonitrile yields a dimer radical anion, $\{CH_3CN\}_2^-$,[19,22,23,28−30] whereas β-acetonitrile yields a monomer radical anion, CH$_3$CN$^-$.[19,29,30] Because no analogous species appear to be formed in the gas phase, it may be inferred that the acetonitrile molecules surrounding these radical anions in the crystal act as a kind of "solvation shell" in the stabilization of these anions.

In $\{CH_3CN\}_2^-$, the spin density is equally divided between the two halves of the dimer anion such that there is hyperfine interaction with pairs of magnetically equivalent nuclei from the two molecules.[19] Thus the structure is centrosymmetric with the two acetonitrile molecules arranged in an antiparallel configuration. Tables 1 and 2 list the principal values of the **g** and hyperfine coupling (hfc) **a** tensors for dimer and monomer radical anions in α- and β-CD$_3$CN, respectively. In Table 1, the directional cosines for the principal axes of these tensors (where known) in single crystal α-acetonitrile are given (after ref 30). Another dimer radical anion with nitrogen hfc param-

TABLE 2: EPR Parameters for Monomer Radical Anions in γ-Irradiated Orthorhombic β-Acetonitrile-d_3 and High-Temperature Phase of Crystalline Adiponitrile-d_8, Both at 77 K (data of ref 46 for HCN^- in KCl are given for comparison); after refs 19 and 30[a]

nucleus	hfcc, isotropic	component	hfcc	hfcc	adiponitrile-d_8[d]	HCN^-[e]
^{14}N	8.17	**aa**	3.5 *(2.9)*	−4.7	0	0
		bb	8.2 *(8.1)*	0	0	0
		cc	12.8 *(12.9)*	4.7	20.9 *(21.1)*	20.9
$^{13}CD_3$ (^1H for HCN^-)	∼88	**aa**				131.3
		bb				136.5
		cc				141.3
^{13}CN[a]	61.4	**aa**	53	−8.4		65.6
		bb	59.6 *(59.4)*	−1.8		68.6
		cc	71.7	10.3		90
g-tensor		**aa**	1.9991 *(1.9992)*		1.9987	2.0005
		bb	2.0031		2.0028 *(2.0025)*	2.0023
		cc	2.0022 *(2.0021)*		2.0018	2.0023

[a] Hyperfine coupling constants (hfcc) are given in Gauss ($1G = 10^{-4}$ T); there are two variants of the monomer in β-acetonitrile, at site-1 and site-2; parameters in italics are given for site-2 (where different from site-1). [b] The **c** axes of the g-, ^{14}N, and ^{13}CN tensors are collinear within 5−7° and point in the same direction for both variants (axis *y*); axes **b**[g] for the two variants lay in the same *xz* plane and make an angle of 75° with each other (ref 30). [d] For adiponitrile-d_8 there are two sites, the g- and ^{14}N hfc tensors are nearly coaxial in both of the variants (ref 30). [e] Ref 46.

eters very similar to those of $\{CH_3CN\}_2^-$ was found in the plastic (α-) and monoclinic (β-) phases of succinonitrile-d_4, $NC(CD_2)_2CN$,[21,22] and in the low-temperature phase of crystalline adiponitrile-d_8, $NC(CD_2)_4CN$.[29,30] All of these dimer anions strongly absorb in the visible: the profile of the absorption bands in acetonitrile and succinonitrile are almost identical with the peak at 530 nm and the onset close to 875 nm.[19,24,25,29]

A monomer anion with EPR parameters and an optical absorption very similar to those found for CH_3CN^- in β-acetonitrile was also observed in the high-temperature phase of adiponitrile-d_8 (Table 2).[30] The absorption peak in the optical band of these monomer radical anion at 430−440 nm is blue-shifted relative to that of the dimer radical anion at 530 nm.[19,29] A transient 450 nm band with the lifetime of 300 ns has also been observed in the pulse radiolysis of solid succinonitrile present in the rotator phase at 295 K,[26] and has been assigned to a monomer radical anion formed shortly after the ionization event. Because the metastable dimer anion is formed in this phase at 77 K, the short lifetime of the 450 nm species at the much higher temperature of 295 K suggests that the monomer anion dissociates before it can combine with another nitrile group to form a dimer anion. This is not surprising given the high mobility of the plastic crystal phase at 295 K.

Photoexcitation of the monomer and dimer radical anions in their respective absorption bands brings about their dissociation to CN^- and the corresponding alkyl radical.[19,20,24,27,29] The same photofragmentation process was observed for anion-1 and anion-2 in liquid acetonitrile.[18] Remarkably, the reverse reaction between methyl radicals and cyanide anions takes place thermally in the crystalline state, this recovery to the radical anion competing with H- or D-atom abstraction by the methyl radicals from neighboring acetonitrile molecules.[19] Because this abstraction reaction occurs largely by quantum-mechanical tunneling at low temperatures,[19] it is subject to a large H/D isotope effect so that complete recovery is observed to the radical anion in acetonitrile-d_3.

It is also of interest that the absorption bands of the dimer radical anions in α-acetonitrile[19,24,29] and α- and β-succinonitrile[25] exhibit well resolved vibronic progressions extending over 13 000 cm^{-1}. For α-acetonitrile, Sprague et al. have reported these vibronic progressions for several H/D isotopomers.[19,29] In addition, angle-resolved EPR spectra are available for α- and β-single-crystal CD_3CN, $^{13}CD_3CN$, and $CD_3{}^{13}CN$;[19,28,29,30] These data (and the analyses of EPR spectra for polycrystalline samples) provided hfc tensors for ^{14}N, $^{13}CH_3$, and ^{13}CN nuclei given in Tables 1S, 1, and 2.

The original studies were analyzed and interpreted in the absence of reliable crystallographic data. These data became available for α-CH_3CN in 1981,[31] for succinonitrile in 1990,[33,34] and for β-CD_3CN in 1992.[32] Capitalizing on the structural insight obtained from these later X-ray and neutron diffraction studies, we are now able to provide a more complete interpretation of the EPR and optical data for these excess-electron centers in solid alkyl cyanides, especially with regard to the controlling influence of crystal structure on the issue of monomer or dimer anion formation.

In addition, the current availability of advanced theoretical methods such as density functional theory (DFT) has allowed us to carry out detailed calculations on the molecular structure of these electron centers, so that a more precise analysis of the experimental data can now be given in terms of well-defined structural models. For example, while several possible antiparallel structures for the dimer radical anions of acetonitrile were discussed more than 20 years ago by Williams and Sprague,[19] and by Egland and Symons,[23] the nature and position of the actual "bonding" interaction between the individual molecules in such a staggered dimeric arrangement could not be reliably determined with the aid of theory at that time. As described herein, a satisfactory resolution of this problem has been achieved through the combined use of the theoretical and experimental data.

Finally, the Fourier transform analysis has been applied to uncover the vibrational frequencies of the fundamental modes contributing to the vibronic structure of the visible absorption bands observed in the dimer radical anions. This provides new information about the character of the orbital transition as well as the change of geometry accompanying the electronic excitation of these dimer anions.

To save space, some data are given in the Supporting Information. Figures and tables with a designator "S" after the number (e.g., Figure 1S) are placed therein.

2. Dimer Radical Anion in α-Acetonitrile

2.1. Crystallography and Orientations of g- and Hyperfine Coupling Tensors. Monoclinic α-acetonitrile (space group $P2_1/c$, $a = 4.11$ Å, $b = 8.27$ Å, $c = 7.98$ Å, and $\beta = 100.42°$) consists of two stacks of antiparallel $\{CH_3CN\}_2$ pairs with the C_{2h} symmetry (Figure 1, on the left).[31] One of these pairs is

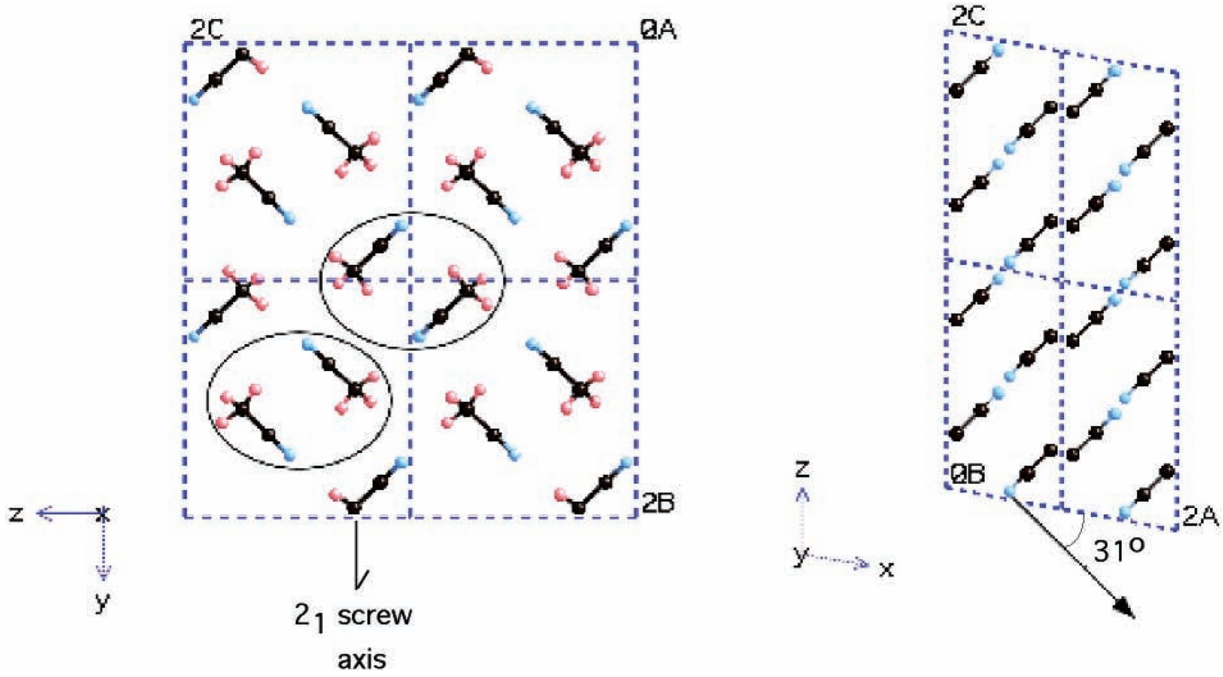

Figure 1. Two views of monoclinic α-CH_3CN, after X-ray diffraction data of ref 31. *On the left:* a view along the short axis **a**; two variants of "antiparallel" $\{CH_3CN\}_2$ pairs are highlighted. These two pairs are transformed to each other by a 2_1 screw rotation in the direction of axis **b**. *On the right:* a view along axis **b** (hydrogens are not shown); all of these $\{CH_3CN\}_2$ pairs lay in the same (−299, ±28, 449) plane whose normal makes an angle of 31.14° with axis **a**.

shown separately in Figure 1S. The $\{CH_3CN\}_2$ pairs are stacked in the direction of the short axis **a** (Figure 1); we identify this direction with the (growth) axis z of α-acetonitrile crystals in the EPR experiments of Williams' group.[28,30] By contrast, orthorhombic β-acetonitrile (space group $Cmc2_1$, a = 5.99 Å, b = 5.21 Å, and c = 7.73 Å) consists of infinite chains of parallel CH_3CN dipoles (section 3).[32]

The two $\{CH_3CN\}_2$ pairs in α-acetonitrile are transformed into each other by a 180° screw rotation around the 2_1 axis (||**b**). These two pairs lie in the same plane (the Miller indices are (−299, ±28, 449); Figure 1, on the right). The normal of this plane makes an angle of 31.14° with the growth axis **a**. If the dimer radical anion retains the overall C_{2h} symmetry and the symmetry plane of the $\{CH_3CN\}_2$ pairs, there would be two variants of the dimer anion whose EPR spectra transformed into each other by a 90° rotation around axis **a.** This is indeed the case.[28,30] According to the angular analyses of Takeda,[30] the EPR parameters for both of these variants are very close (Table 1S) suggesting that these two variants are magnetically equivalent. As explained in refs 19 and 28, the **b** axis of the g-tensor (that corresponds to the largest prinicipal value, Table 1) must be in the direction normal to the symmetry plane. One of the principal axes of the hfc tensors should also point in that direction. A glance at the stereographic projection of the principal axes for the g- and hfc tensors shown in Figure 2S(a) suggests that for carbon-13 in the methyl groups, this must be the **b** axis, since the corresponding **a** and **c** axes lay in the same plane as the long **c** axis of the hfc tensor of nitrogen-14. The data of Table 1, indicate that the **b**[g] and **b**[$^{13}CD_3$] axes make, respectively, angles of 33° and 34° with the crystallographic axis **a**; these two estimates are very close to 31.14° for the crystallographic $\{CH_3CN\}_2$ pairs. For the two variants of the $\{CD_3CN\}_2{}^-$ anion in α-CD_3CN, the directions of the **b** axes of the g tensors are coincident and their **c** axes are transformed to each other by a 74° rotation about these **b** axes (Table 1S and Figure 2S(b)).[30] This angle is close to the angle of 72.5° by which one crystallographic $\{CH_3CN\}_2$ pair is transformed into another by rotation in the symmetry plane.

Further inferences about the geometry of the dimer radical anion can be made from the orientation of the long (**c**) axes of the $^{13}CD_3$ and ^{14}N tensors (Figure 2S). The **c**[^{14}N] axis is nearly coaxial with the **c**[g] axis of the g-tensor (within 4−5°). The latter axis corresponds to the principal value that is most close to that of a free electron, 2.0023. Therefore, this is the direction of the spin-bearing N 2p orbital, perpendicular to the CN bond. Note, that the principal axes **a**[g], **c**[g], **c**[^{14}N], **c**[$^{13}CD_3$], and **a**[$^{13}CD_3$] all lie in the same plane, as would be expected for the ^2A_g or ^2B_u state of the dimer anion with the C_{2h} symmetry. For methyl carbon-13, the long axis **c** should be in the direction of the C 2$p\sigma$ orbital, i.e., in the direction of the C−CD_3 bond. If the C−C≡N fragment were linear, the long **c** axes of the ^{14}N and $^{13}CD_3$ hfc tensors would make a right angle. According to Table 1, the actual angle is close to 56° (site-1; for site-2, this angle is 51.4°). This suggests that the CCN fragment is bent. This conclusion is further supported by the fact that the **a**[g] axis does not point in the same direction as either **a** or **c** axis of the hfc tensor for $^{13}CD_3$. A crude estimate of the CCN angle is $90° + 56° \approx 146°$.

In sum, the EPR data clearly point to a dimer radical anion with C_{2h} symmetry; the state symmetry representation being either ^2A_g or ^2B_u. This dimer radical anion lies in the same crystallographic plane as the original $\{CH_3CN\}_2$ pair and involves two bent acetonitrile molecules. The two variants of the dimer anion have nearly the same relative orientation as the two crystallographic $\{CH_3CN\}_2$ pairs.

Crystallographic data of refs 31−34 suggest that preexistence of the antiparallel $\{RCN\}_2$ pair is required for the formation of the *dimer* radical anion. No such anions are formed in β-acetonitrile where such pairs are lacking. In cubic α-succinonitrile (a = 6.34 Å) that yields dimer radical anions upon γ-irradiation,[19−22] the cyanide nitrogens occupy any one of the face centers, and both *trans*- and *gauche*- isomers of $NC(CH_2)_2$-

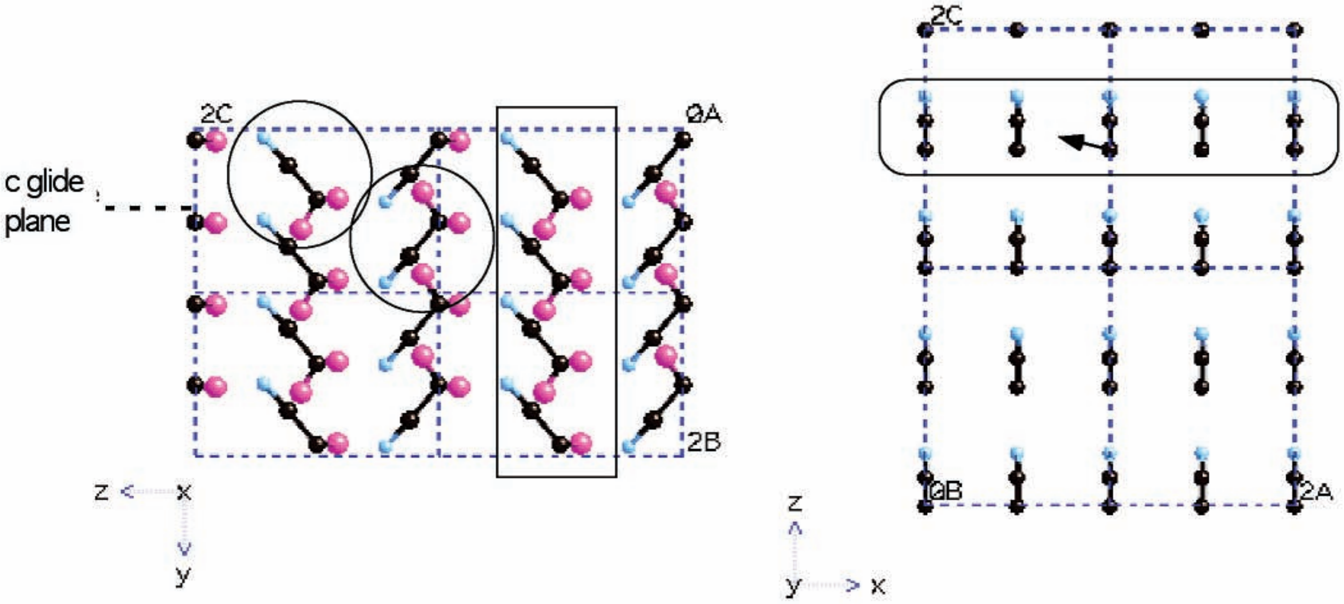

Figure 2. Two views of orthorhombic β-CD_3CN, after neutron diffraction data of ref 32. *On the left:* a view along axis **a**; there are two kinds of "parallel" $\{CH_3CN\}_\infty$ chains in the direction of this axis (highlighted by ovals). These chains occupy (0, ±345, −580) planes and transform to each other by **c** glide reflection in the (010) plane (indicated). The cyanide groups lay in the (100) plane. There are also "parallel" chains pointing in the direction of the (1,1,0) vector (one of them is highlighted by a rectangle, see also Figure 5S). *On the right:* a view along the short axis **b** (the D atoms not shown); one of the chains is highlighted. The arrow indicates the direction of CCN bending upon electron attachment (see section 3).

CN occur (see, for example Figure 1 in ref 34 and Figures 1 and 2 in ref 33). Although there are many different configurations for the nearest neighbors,[33] the *trans*−*trans* pair with the C_{2h} symmetry is favored energetically (Figures 3S and 4S).[33,34] The atomic-resolution structure of the monoclinic (β-) phase that is stable below 236 K is not known, but it is likely that this crystal consists of the *trans* molecules which have the lowest conformation energy. Perhaps, the crystal structure of β-succinonitrile is similar to that of the monoclinic α-acetonitrile. Both phases of succinonitrile yield dimer radical anions whose EPR[21,22,25] and optical[25] spectra are identical. Thus, the structure of the dimer anions in these two phases must be the same. The EPR parameters of the dimer anion in α-succinonitrile are very similar to those for $\{CH_3CN\}_2^-$ in α-acetonitrile suggesting that the spin densities and the orientation of the CCN fragments are similar. The crystallographic data of ref 33 indicate that the distance between the linear C−C≡N fragments of the *trans*−*trans* pair shown in Figure 4S and is 3.93 to 4.03 Å which is considerably longer than this distance for the $\{CH_3CN\}_2$ pair in α-acetonitrile[31] (3.48 to 3.53 Å, Figures 1 and 1S) but is similar to that in β-acetonitrile (∼3.97 Å, Figures 2 and 5S).[32] This example demonstrates that it is the *antiparallel orientation* of the neighboring C−C≡N fragments rather than the distance between these fragments that determines whether a dimer or a monomer radical anion is formed in a nitrile crystalline phase.

2.2. Vibronic Progressions. The dimer anions in γ-irradiated α-acetonitrile and α-succinonitrile (77 K) exhibit well resolved vibronic progressions in the 850−400 nm region (see, for example, Figure 3 in ref 19, Figure 1 in ref 24, and Figure 1 in ref 25). The original data of refs 25 and 29 were analyzed in the following way: the VIS spectra were fit by a polynomial using the least-squares optimization, and the residue obtained after the subtraction of this polynomial (Figure 6S) was Fourier transformed (FT). Figure 3 demonstrates power FT spectra obtained for several isotopomers of acetonitrile; the positions of the strongest peaks are listed in Table 3. More elaborate interpretation of these FT spectra will be given below, as it requires a knowledge of the dimer radical anion structure. Here, we summarize the most important features.

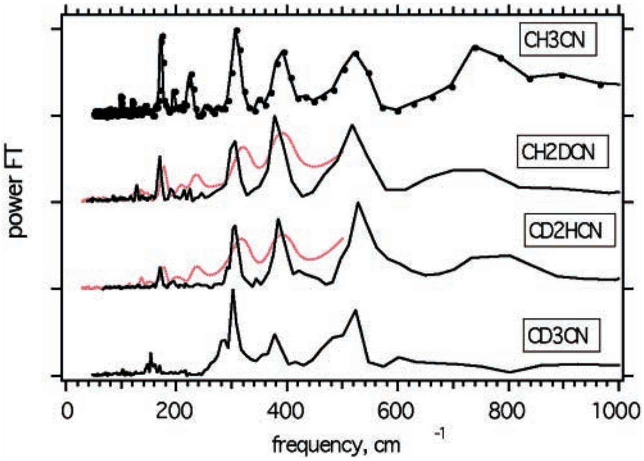

Figure 3. Power FT spectra of vibronic progressions in the $^2B_u \leftarrow {}^2A_g$ absorption band of the dimer radical anions in γ-irradiated low-temperature α-acetonitrile (the isotopomers are indicated in the figure next to the traces). The dotted lines were obtained from the 600−900 nm scans; the bold traces were obtained from the 400−750 nm scans. See refs 19 and 29 for more detail.

TABLE 3: Main Vibration Modes in the Vibronic Progressions for Dimer Radical Anion Observed in γ-Irradiated Monoclinic α-Acetonitrile and Cubic α-Succinonitrile at 77 K (after Figures 3 and 7S)

crystal	vibration modes, cm^{-1}
CD_3CN	152, 302, 387, 483, 522, 617?, 754?
CD_2HCN	171, 232?, 307, 383.6, 527.5, 773
CH_2DCN	170, 232?, 307, 378, 517, 720 ± 20
CH_3CN	172, 224, 307, 392, 483, 533, 767
$NC(CH_2)_2CN$	142, 229, 310, 390, 501?

First, only skeletal vibrations in the fundamental range are represented in these FT spectra: all of the modes have frequencies below 800 cm^{-1}. In the CH_3CN/CD_3CN monomer,[35] the two low-frequency modes are the C−C stretch (920/831 cm^{-1}) and the C−C≡N bend (361/331 cm^{-1}). In liquid acetonitrile, a 75 cm^{-1} vibration was observed for the breathing mode of the antiparallel molecular dimer.[36]

The FT spectra for the dimer radical anion in α-CH_3CN are dominated by the modes with frequencies ∼307, 380, and 520 cm^{-1}. These frequencies change little (2−3%) on the H/D substitution in the methyl group (Table 3). Therefore, these three modes are associated with the vibrations of the CCN fragment. The 310 and 390 cm^{-1} modes were also observed in α-succinonitrile (Figure 7S), whereas the 500 cm^{-1} mode is very weak. Judging from the signal intensities, this 500 cm^{-1} mode is red-shifted to 400 cm^{-1}. The fact that the same modes occur upon H/D substitution and derivatization of the methyl group indicates that these are the CCN bending modes. Because no anion with a linear CCN fragment can have that many bending modes, the immediate conclusion is that the CCN fragment is bent (that is, in the excited state which yields the vibronic progression). This finding is consistent with the EPR results for the bent ground-state geometry of the dimer radical anion.

A relatively strong isotope effect (12%) is observed for the lowest-frequency 172 cm^{-1} mode in α-CH_3CN; this mode changes to 142 cm^{-1} in α-succinonitrile (cf. Figures 3 and 7S). A broad 720−770 cm^{-1} peak observed in CH_3CN, CHD_2CN, and CDH_2CN is lacking in α-CD_3CN and α-succinonitrile. It is likely that this peak corresponds to a combined mode.

2.3. *Ab Initio* Modeling of $\{CH_3CN\}_2^-$. In this section, a structure for the $\{CH_3CN\}_2^-$ dimer is suggested that (i) accounts for the observed EPR parameters, (ii) yields the absorption band with an onset at 1.45 eV, and (iii) rationalizes the vibronic progressions examined above.

To this end, several likely structures were examined using *ab initio* methods from *Gaussian 98* (Gaussian)[37] and *Spartan* (Wavefunction, Inc.) quantum chemistry packages. Two methods were mainly used: unrestricted Hartree−Fock (UHF) calculation followed by a Møller−Plesset correlation energy correction truncated at second-order (MP2)[38] and density functional theory (DFT) model with Becke's exchange functional[39] and Lee−Yang−Parr correlation functional[40] (B3LYP). The C_{2h} symmetry of the dimer anion has been imposed in all of these calculations. Other DFT methods were also used, e.g., the model with Slater exchange functional[41] and Vosko−Wilk−Nusair correlation functional[42] (SVWN or LSDA, depending on the formulation of the functionals). We found it important that the calculation method includes at least some correction for the correlation energy, otherwise, the hfc constants are inconsistent with those in Table 1. In some DFT calculations, the effect of the "solvent" (liquid acetonitrile) has been included using polarized continuum method of Tomasi et al.,[43] this method was used in the integral equation formulation given in refs 43 (IEFPCM). The basis sets used in these calculations varied from the tight-binding 3-21G(s,p) set to extended sets that included polarization (6-31G, DN) and diffuse (6-31+G**) functions. In some cases, a specialized double-ζ basis set optimized for DFT calculations of hfc constants (EPR-II) was used;[44] the hfc constants obtained using this basis set were similar to those obtained using 6-31G and 6-31+G** basis sets. In fact, the optimized geometry and hfc constants varied little between the computation methods and the basis sets. A reasonable guess for the dimer anion geometry can be obtained using UHF and even semiempirical[37] methods.

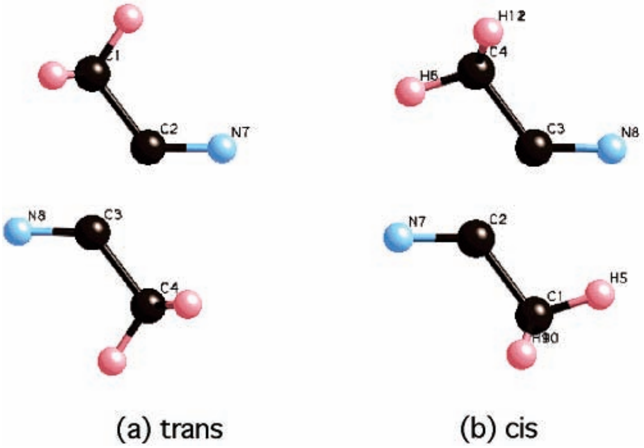

Figure 4. Optimum geometry *trans*- (a) and *cis*- (b) conformers of $\{CH_3CN\}_2^-$ obtained in a DFT calculation using B3LYP/6-31+G** method. We use *trans*- and *cis*- to specify the in-plane directions of the methyl hydrogens with respect to each other (away and toward, respectively). For the conformations of the individual molecules, the in-plane methyl hydrogens are *syn*- with respect to the CN group in the *trans*-dimer and *anti*- in the *cis*-dimer. See Tables 4 and 5 for the angles and bond lengths.

Figure 4 shows the optimum geometry for $\{CH_3CN\}_2^-$ dimer anion obtained using the B3LYP/6-31+G** method. For both *cis*- and *trans*-conformers, the lowest energy state is the ^2A_g state. In *trans*-$\{CH_3CN\}_2^-$ (Figure 4(a)), the in-plane methyl hydrogens point away from the cyanide nitrogen; this is the conformation of methyl groups in the crystallographic $\{CH_3CN\}_2$ pair shown in Figures 1 and 1S. In *cis*-$\{CH_3CN\}_2^-$ (Figure 4(b)), this methyl hydrogen points toward the cyanide nitrogen, forming a week hydrogen bond (the N−H distance is ∼2.17 Å); this is the conformation of methyl groups in the gas-phase $\{CH_3CN\}_2$ dimer.[12] The bond lengths and angles obtained for these conformers are given in Tables 4 and 5. In the DFT and MP2 calculations with tight-binding sets, the *cis* conformer is 100−120 meV more stable than the *trans* conformer. In the DFT calculations with extended basis sets, these two conformers are within 10−20 meV of each other (Table 5). Because the calculated parameters (such as hfc tensors and optical transitions) for both of these conformers are similar, our results do not indicate which one of these occurs in α-acetonitrile. Perhaps, it is the *trans* conformer since no rotation of methyl groups following electron attachment is needed in such a case.

In these dimer anions, the negative charge and the spin density are mainly in the methyl carbon and cyanide nitrogen. According to the LDSA/VWR/DN calculation for *cis*-$\{CH_3CN\}_2^-$, the electrostatic charges on these C and N atoms are −0.594 and −0.769, respectively (vs −0.24 and −0.42 in CH_3CN), in electron units. In the B3LYP/6-31+G** calculation (Figure 4(b)), the Mulliken charges on these C and N atoms are −0.518 and −0.522, respectively, and the total atomic spin densities are 0.116 and 0.467, respectively. The largest spin density resides on the N atoms; this is why the direction of the **c** axis of the g tensor is that of the spin-bearing N 2*p* orbital (which is also the direction of the long axis of the ^{14}N hfc tensor, Table 1 and Figure 2S). Although the exact geometry of the dimer anion varies for different computation methods (Tables 4 and 5), several trends persist:

(i) There is a pseudo bond between the cyanide carbons, C_2-C_3 (in the numbering scheme of Figure 4). The bonding a_g SOMO is shown in Figure 5b. The length of the C_2-C_3 bond is estimated to be between 1.65 Å and 1.8 Å, depending on the computation method. Calculations with extended sets yield shorter C_2-C_3 bonds. All other properties strongly depend on the length of this bond. For example, the hfc tensors obtained for the optimum-geometry structure using the B3LYP/6-

TABLE 4: Optimum Geometries, EPR Parameters, and Optical Transitions for the Ground ^2A_g State of *cis*-$\{CH_3CN\}_2^-$ Anion (the atoms are numbered after Figure 4(b))

parameter[a]	B3LYP	B3LYP IEF PCM[c]	B3LYP	B3LYP IEF PCM[c]	B3LYP	B3LYP	SVWN5	SVWN	LSDA VWN[d]	MP2
basis set	3-21G	3-21G	6-31G	6-31G	6-31+G**	EPR-II	6-31G	3-21G	DN	3-21G
C2−N7	1.231	1.231	1.250	1.25	1.234	1.241	1.260	1.243	1.253	1.211
C1−C2	1.532	1.528	1.526	1.523	1.526	1.534	1.509	1.513	1.503	1.542
C1−H5	1.099	1.098	1.099	1.098	1.097	1.097	1.118	1.122	1.11	1.097
C1−H9	1.0988	1.098	1.099	1.098	1.097	1.096	1.108	1.106	1.11	1.097
C2−C3	1.782	1.774	1.677	1.671	1.708	1.686	1.605	1.653	1.609	1.813
∠C1−C2−N7	132.4	132.3	127.5	127.4	127.6	127.1	127.7	131.5	127	134.9
∠C2−C1−H5	106.3	106.7	107.9	108.2	109	108.3	105.3	103.3	110.7	106.2
∠C2−C1−H9	110.8	111	110.9	111	110.1	110	111.3	111.3	111	110.1
∠H9−C1−C2−N7	59.9	59.9	59.6	59.6	59.3	59.5	60	60.4	59.7	59.8
∠C1−C2−C3	106.2	106.8	110.4	111	110.7	110.7	110.3	106.9	106.9	104.9
^{14}N[7], iso	6.16	6.22	8.1	8.15	6.3	4.96	5.98	4.36		
aa	−6.4	−6	−6.8	−7.3	−6.95	−7.5	−6.6	−5.8		
bb (z)	−5.2	−4.9	−5.6	−6	−5.95	−6.3	−5.7	−5.1		
cc	11.7	11	12.5	13.3	12.9	13.8	12.2	10.9		
^{13}C[1]H$_3$, iso	14.3	13.3	14.2	13.3	15.3	14.82	8.97	6.94		
aa (z)	−2.9	−2.7	−2.9	−2.9	−2.8	−2.9	−2.9	−2.9		
bb	−2.5	−2.3	−2.5	−2.6	−2.4	−2.6	−2.5	−2.5		
cc	5.4	5.1	5.4	5.4	5.2	5.5	5.4	5.5		
^{13}C[2]N, iso	−1.3	−2	−2.3	−3.06	−2.7	−2.9	5.71	6.09		
aa (z)	−3.3	−3.4	−4	−4	−3.8	−3.9	−3.8	−3.5		
bb	−0.8	−0.7	−0.6	−0.5	−0.75	−0.8	−0.2	−0.3		
cc	4.1	4.1	4.5	4.5	4.6	4.7	4	3.9		
∠**c**[N],**c**[CH$_3$]	73.8	72.8	67.9	66.9	65.3	63.9	73.7	79.8		
$^2B_u \leftarrow {}^2A_g$, eV	2.342		1.42		1.394					2.67
osc. strength	0.080		0.071		0.096					0.081
ΔG_{solv}[c]		−2.0		−2.06						

[a] The bond lengths are given in Å, and the angles in degrees; hfc constants in Gauss; the energies in eV; the *z* axis is normal to the symmetry plane. [b] Computation methods from Gaussian 98 (ref 37). [c] IEFPCM method of Tomasi et al. (ref 43); ΔG_{solv} is the free energy of anion solvation estimated in this model. [d] A DFT method from Spartan.

31+G** method may also be obtained using the B3LYP/3-21G method provided that the short-bond geometry given by the former method is retained (this is clearly seen from a comparison of the data in Table 4 and Figures 12S and 13S, see below).

(ii) The CCN fragment in the monomer subunits is bent. The CCN angle is estimated to be between 128° and 135°, depending on the computation method. The models yielding shorter C_2-C_3 bond yield smaller CCN angles. As anticipated, the **c**[$^{13}CH_3$] axis is in the direction of the C 2$p\sigma$ orbital along the $C-CH_3$ bond (Figure 5), whereas the **c**[^{14}N] axis points in the direction of the N 2*p* orbital perpendicular to the C−N bond. A typical juxtaposition of the in-plane principal axes of hfc tensors for the ^{13}C and ^{14}N nuclei is shown in Figure 8S. The same models that yield smaller CCN angles also yield more acute angles between the **c**[^{14}N] and **c**[$^{13}CH_3$] axes. The lowest ∠{**c**[^{14}N],**c**[$^{13}CH_3$]} angle, 60−63°, was obtained for *trans*-$\{CH_3CN\}_2^-$ in the B3LYP/6-31G and B3LYP/6-31+G** calculations (Table 5). These estimates compare favorably with 58° obtained for this angle from the data of Table 1.

(iii) The C−N and $C-CH_3$ bonds in the dimer anion are stretched. The crystallographic distances for these two bonds are 1.13 Å and 1.443 Å, respectively.[31] The B3LYP/3-21G calculation for the neutral $\{CH_3CN\}_2$ dimer yields 1.16 Å and 1.46 Å, respectively (and C_2-C_3 of 3.31 Å). By contrast, the C−N bond in the dimer anion is 1.21 to 1.25 Å, and the $C-CH_3$ bond is 1.51 Å to 1.54 Å (Tables 4 and 5). The calculations that yield longer C_2-C_3 bonds yield shorter C−N and $C-CH_3$ bonds (see also Figure 6(b) and 11S).

(iv) Both the isotropic (Fermi) hfc constants and the dipole hfc tensors (Tables 4 and 5) obtained using DFT method compare favorably with those given in Table 1; the *cis*-conformer in the B3LYP/6-31+G** calculation (Table 5) gives the best match. The only major disagreement is the reversal of the **aa** and **bb** components for methyl carbon. Because the corresponding hfc tensor is almost axial, this reversal could be due to crystal field effects. Note, that inclusion of the "solvent" has little effect either on the optimum geometry or the hfc constants (Table 4). Gillbro et al.[28] estimated that the isotropic hfc for methyl protons are ∼2 G (1 G = 10^{-4} T). The B3LYP/6-31+G** calculation for *cis*-conformer gives −2.5 G and −1.1 G for the in-plane and out of plane methyl protons, respectively.

(v) Using the configuration interaction method with single-electron excitations (CIS)[45] and MP2 electron density, the electronic transitions of the optimized-geometry dimer anions have been estimated (Tables 4 and 5). The ^2B_u is the first and ^2B_g is the second excited state near the bottom of the potential well for the ground ^2A_g state (Figure 9S). The $^2B_u \leftarrow {}^2A_g$ transition results from the excitation of the electron from a doubly occupied b_u (in-plane) molecular orbital No. 22 to a singly occupied a_g molecular orbital No. 23 (these MO's are shown in Figure 5a and 5b, respectively); the difference in the energies for these two orbitals is ≈2 eV. This electronic transition is allowed by symmetry, and the oscillator strength is 0.07−0.096. According to the MP2 and CIS calculations shown in Figure 9S, the ^2B_u term (plotted as a function of the C_2-C_3 distance) is steep. Consequently, the calculation methods that yield shorter C_2-C_3 distances (for extended basis sets) locate this transition at lower energy (Tables 4 and 5). The CIS calculation using B3LYP density locates the $^2B_u \leftarrow {}^2A_g$ transition at 1.42 eV (6-31G basis set) or 1.394 eV (6-31+G** basis set), respectively, which is close to the experimental estimate for the onset of the 530 nm band, 1.45 eV. The optimum-geometry ^2B_u state (shown in Figure 10S) exhibits shorter C_2-C_3 bond (1.43 Å vs 1.81 Å), smaller CCN angle

TABLE 5: Optimum Geometries, EPR Parameters, and Optical Transitions for the Ground ^2A_g State of *trans*-$\{CH_3CN\}_2^-$ and $\{$*trans*-$NC(CH_2)_2CN\}_2^-$ (the atoms are numbered after Figure 4(a))[a]

parameter	B3LYP	B3LYP	B3LYP	MP2	B3LYP[b]
basis set	3-21G	6-31G	6-31+G**	3-21G	3-21G
E(*trans*) − E(*cis*)	0.104	0.011	−0.023	0.129	
C2−N7	1.233	1.251	1.234	1.216	1.235
C1−C2	1.533	1.525	1.524	1.544	1.534
C1−H5	1.097	1.096	1.095	1.097	
C1−H9	1.097	1.098	1.097	1.094	1.095
C2−C3	1.739	1.657	1.692	1.747	1.69
∠C1−C2−N7	131.4	127.7	128.2	133.3	129.2
∠C2−C1−H5	110.8	110.4	110	109.5	
∠C2−C1−H9	109.2	110	109.8	109.2	
∠H9−C1−C2−N7	−122.1	−121.8	−121.7	−121.5	
∠C1−C2−C3	106.3	110.2	110	105.6	
^{14}N[7], iso	6.36	8.1	6.24		6.24
aa	−6.5	−7.2	−6.9		−6.3
bb (z)	−5.3	−6	−5.9		−5.2
cc	11.8	13.3	12.8		11.5
^{13}C[1]H_3, iso	18.9	17.66	19.0		17.5
aa (z)	−2.5	−2.5	−2.6		−2.4
bb	−2.1	−2	−2		−2.1
cc	4.6	4.5	4.6		4.5
^{13}C[2]N, iso	1.58	0.59	−0.82		2.82
aa (z)	−3.7	−4	−3.9		−3.5
bb	−1.1	−0.8	−0.9		−1.1
cc	4.7	4.9	4.9		4.5
∠**c**[N],**c**[CH_3]	63.9	61	60.8		60.7
$^2B_u \leftarrow {}^2A_g$ transition energy	1.933	1.41	1.276	2.287	
osc. strength	0.0772	0.080	0.0865	0.094	

[a] The bond lengths are given in Å, and the angles in degrees; hfc constants in Gauss; energies in eV; the computation methods are from Gaussian 98; the z axis is normal to the symmetry plane. [b] Selected parameters for $\{$*trans*-$NC(CH_2)_2CN\}_2^-$ (Figure 14S; the atoms in the CCN fragments are numbered after Figure 4(a)).

(120.5° vs 134.9°), and longer $C-CH_3$ bonds (1.57 Å vs 1.55 Å) than the ground ^2A_g state (MP2/3-21G calculation). The antibonding character of the b_u orbital and considerable elongation of the $C-CH_3$ bond accounts for the spontaneous fragmentation[18−21] of this excited state to CH_3 and CN^- (in our model, this dissociation cannot be simulated due to the imposed C_{2h} symmetry). Even at longer C_2-C_3 distances, the ^2B_u state exhibits stronger C−C stretching and CCN bending than the ^2A_g state (Figure 11S). These trends can be understood using simple MO considerations presented in section 2.4.

(vi) Figures 6(a) and 9S(b) show the potential energy surfaces for the ground ^2A_g state of *cis*-$\{CH_3CN\}_2^-$ calculated using B3LYP/3-21G and MP2/3-21G methods, respectively. In this calculation, the C_2-C_3 distances were varied between 1.3 Å and 2.9 Å while other bond lengths and angles were optimized. For C_2-C_3 distances larger than 2.9 Å, the ^2A_g state is no longer the ground state. For the dimer anion that has the geometry of the crystallographic $\{CH_3CN\}_2$ pair, the lowest state is ^2B_g. As the C_2-C_3 distance increases, the $C-CH_3$ bond becomes shorter (eventually approaching 1.46 Å, as in the neutral dimer) and the CCN fragment opens to 155−165° (Figures 6(b) and 11S).

The reduction of the C_2-C_3 bond from 2.9 Å to 1.8 Å lowers the energy by 0.4−0.6 eV (Figures 6(a) and 9S(b)). These calculations suggests that the formation of the “figure-8” dimer anion with a short C_2-C_3 bond is energetically favorable and occurs spontaneously once the intermolecular distance is reduced to ∼3 Å (vs 3.3−3.5 Å in the neutral $\{CH_3CN\}_2$ dimer). This initial contraction can only occur via the stabilization of the dimer anion due to polarization of the medium. This polarization energy is large: according to the IEF PCM calculation, the free energy of solvation of the dimer radical anion in liquid acetonitrile is ca. −2 eV. In the gas phase, the $\{CH_3CN\}_2$ dimer strongly repulses the electron.[8] Our B3LYP/3-21G calculation places the lowest state of the dimer anion (retaining the geometry of the neutral dimer) ca. 1.1 eV higher than that of the “figure-8” ^2A_g state. This means that the adiabatic electron affinity of the $\{CH_3CN\}_2$ dimer in the gas phase is negative.

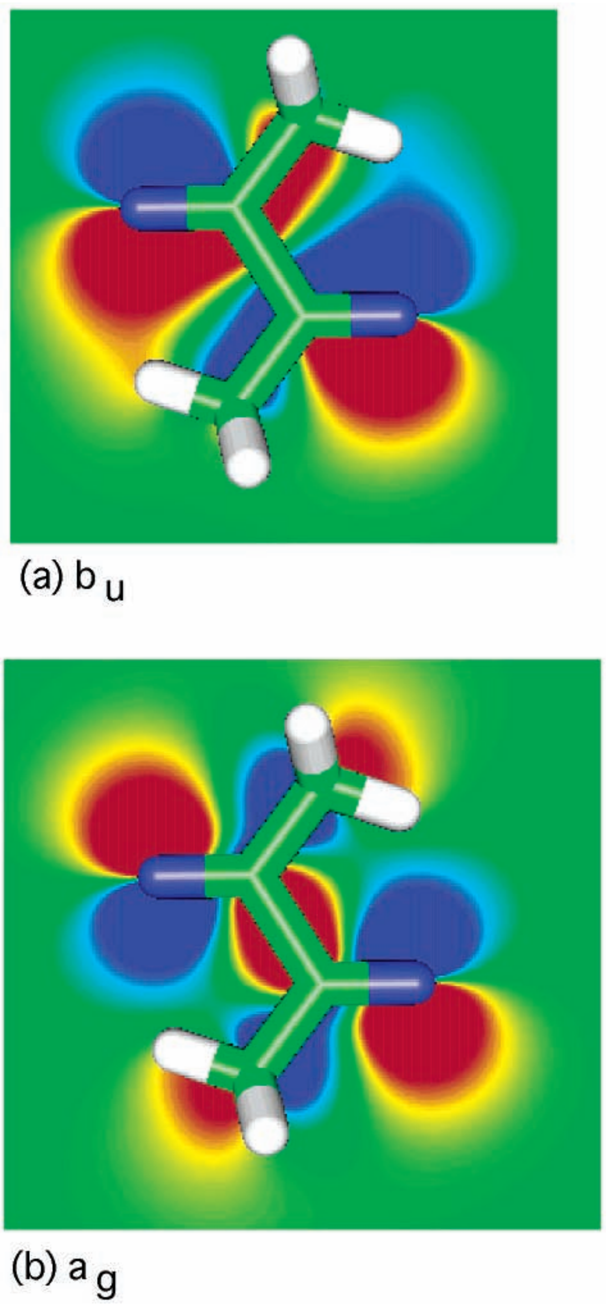
(a) b_u

(b) a_g

Figure 5. Maps of (a) the doubly occupied subjacent b_u MO No. 22 and (b) the spin-bearing singly occupied molecular orbital (SOMO) No. 23 for *cis*-$\{CH_3CN\}_2^-$ obtained in a DFT calculation using B3LYP/6-31+G** method.

Remarkably, the principal values for dipole hyperfine coupling tensors change very little over the entire range of the C_2-C_3 distances (Figure 12S). This explains, why different calculation methods yield very similar estimates for these tensors. By contrast, the isotropic hfc constants change markedly (Figure 13S(a)) as a function of the C_2-C_3 distance, and a

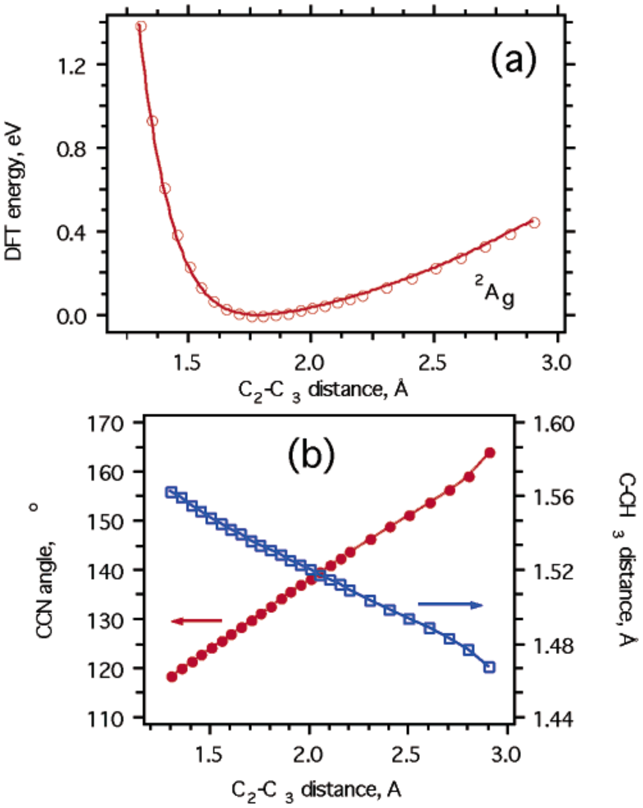

Figure 6. (a) Energy of the ground ^2A_g state of *cis*-$\{CH_3CN\}_2^-$ obtained in a DFT calculation using B3LYP/3-21G method. The DFT energy is plotted vs the C_2-C_3 distance (see Figure 4); all other bond lengths and angles were optimized with assumption of the C_{2h} symmetry. The zero energy corresponds to the lowest energy ^2A_g state. (b) Optimum CCN angles *(filled circles)* and $NC-CH_3$ distances *(open squares)* for the ^2A_g states calculated as stated above. As the C_2-C_3 distance increases, the CCN fragment becomes more linear and $NC-CH_3$ distance approaches the crystallographic value of 1.443 Å (ref 31).

reasonable fit can only be obtained for the short C_2-C_3 distances (1.65−1.7 Å). As discussed above, similarly short C_2-C_3 distances are needed to obtain the correct estimate for the onset of the $^2B_u \leftarrow 2A_g$ transition. Furthermore, as shown in Figure 13S(b), the angle between the **c**[$^{13}CH_3$] and **c**[^{14}N] tensor axes rapidly increases with the C_2-C_3 distance (due to the concurrent increase in the CCN angle), eventually approaching 90°. Because the experiment yields an acute angle of 58°,[30] the C_2-C_3 bond must be short. In sum, the short C_2-C_3 distances obtained in the DFT calculations with extended basis sets are supported by the experiment.

Figure 14S shows the optimum geometry obtained for the ^2A_g state of $\{$*trans*-succinonitrile$\}_2^-$ (in the same conformation of the methylene chain and C_{2h} symmetry as that of the neutral pair shown in Figure 4S). For this structure, the geometry of the CCN fragments and EPR constants are very similar to those for the ^2A_g state of *trans*-$\{CH_3CN\}_2^-$ (Table 5). This is consistent with the EPR data of Bonin et al.[21,22] As in $\{CH_3CN\}_2^-$, the excess negative charge is localized on the coupled CCN fragments. The bond lengths in the outer $NC-CH_2^-$ groups change little: the H_2C-CH_2 and C−N bonds in the dimer anion are 1.55 Å and 1.116 Å vs 1.541 Å and 1.115 Å for the molecule in the crystal, respectively. The distance between the outermost N_3 and N_{18} atoms is 11 Å (Figure 14S). The crystallographic N_3-N_{18} distance for the pair shown in Figure 4S is 10.04 Å, i.e., the accommodation of the structure shown in Figure 14S by the crystal could result in some strain. This may explain why a short-lived monomer anion is observed in the pulse radiolysis of room-temperature α-succinonitrile.[26]

We turn now to the vibronic progressions observed in the $^2B_u \leftarrow 2A_g$ band of the dimer radical anion in α-acetonitrile (section 2.2). These originate in the vibrations of the ^2B_u state: the sample temperature is too low for thermal excitation of the ground ^2A_g state. However, it is difficult to locate this ^2B_u state exactly because it is known to be dissociative.[19] For this reason, we limited ourselves to a calculation of the normal vibration modes for the lowest ^2A_g and ^2B_u states. If not stated otherwise, the frequencies are estimated using B3LYP/3-21G method. Given the uncertainties mentioned above, the use of more computationally demanding methods is not justified.

The IR spectra calculated for ^2A_g state isotopomers ($\{CH_3CN\}_2^-$ and $\{CD_3CN\}_2^-$) of *cis*- and *trans*-dimer anions are shown in Figure 15S; the frequencies of normal modes shown in this figure are listed in Table 2S. For comparison, the normal modes calculated for the $\{CH_3CN\}_2$ dimer are also given. The *cis*-conformer provides the best match for the observed frequencies, and only this conformer is discussed below.

Only b_u and a_u modes contribute to the IR spectra shown in Figure 15S; these two modes are allowed by symmetry. The strongest signals are from the C−H stretch vibrations; the corresponding modes exhibiting a large isotope effect (∼30%). An equally large isotope effect is obtained for CH_3 deformation modes around 1500 cm^{-1}. The skeletal modes with frequencies below 1000 cm^{-1} exhibit much smaller isotope effects (5−7%). Two antisymmetric (in respect to the C_2 axis) CCN bending b_u modes dominate the IR spectrum: 295 and 513 cm^{-1}. In addition, there are two symmetric CCN bending a_g modes, at 402 and 512 cm^{-1}. The frequencies of these four modes compare favorably with the frequencies corresponding to the strongest peaks in Figure 3 (see Table 3). We recall that both the IR-allowed and IR-forbidden modes may be present in the vibronic progression. A correlation diagram in Figure 6S shows how the frequencies of these normal modes change upon the H/D substitution in the methyl groups. It is seen that the lower and the higher a_g and b_u bending modes "change places" upon this H/D substitution, whereas the frequency of the 400 cm^{-1} a_g bending mode decreases by 10%. The net result is that the central section of the spectrum changes little, which is observed experimentally (Figure 3). The out-of-plane a_u mode at 191 cm^{-1} shows a large isotope effect (decreasing to 155 cm^{-1}), see Figure 16S and Table 3S. A similar isotope effect is observed for the 229 cm^{-1} mode in the FT spectrum of $\{CH_3CN\}_2^-$ (Table 3 and Figure 3).

Table 2S lists the normal modes for the lowest-energy ^2B_u state of the two *cis* isotopomers. The IR spectra calculated for the ^2A_g and ^2B_u states are given in Figure 17S; the corresponding normal modes are compared in Figure 18S. Although the geometries of the ground and the first excited states are different, the frequencies of the CCN bending modes in the 300−500 cm^{-1} region do not change significantly: the two b_u modes are at 297 and 532 cm^{-1} and the a_g mode is at 412 cm^{-1} (Tables 2S and 3S). The persistence of these bending modes validates the use of the calculations for the ^2A_g state. Actually, better matching of the vibration modes may be obtained using the diagram shown in Figure 19S in which the frequencies of the normal modes in the ^2A_g state are plotted as a function of the C_2-C_3 distance. The bond length of 1.65 Å provides the best fit of the vibration frequencies. As discussed above, there are other reasons to believe that this C_2-C_3 distance is relatively short.

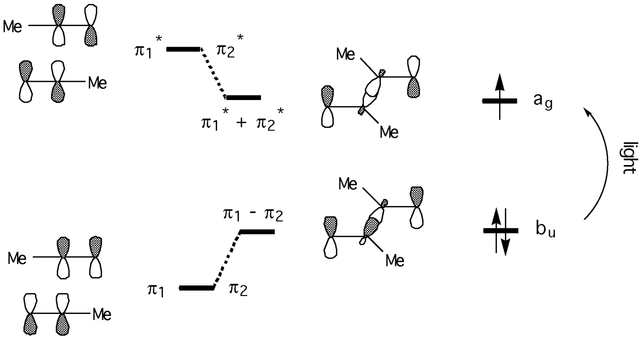

Figure 7. Correlation diagram that indicates how the in-plane π and π* orbitals of the two initially linear acetonitrile molecules interact to yield b_u and a_g orbitals of the dimer radical anion (see the text for explanation).

In Figure 20S, we compare the normal modes for the ^2A_g states of *cis*- and *trans*-$\{CH_3CN\}_2^-$ and $\{$*trans*-$NC(CH_2)_2CN\}_2^-$ anions. It is seen that the a_g and b_u modes with frequencies 500 cm^{-1} are red-shifted in the latter, in agreement with Figure 7S. This occurs due to mixing of the CCN bending modes in the coupled and loose CCN fragments. It is also seen that the 200 cm^{-1} a_u mode is replaced with several lower-frequency modes; the highest-frequency vibration in this group is the a_g mode at 120 cm^{-1} (cf. with the 142 cm^{-1} mode in Figure 7S). Although this analysis is necessarily crude, it appears to be capable of qualitative explanation of the observed trends.

In sum, the staggered side-by-side structures shown in Figure 4 account for most nuances of the EPR and optical spectra for the dimer radical anion observed in γ-irradiated frozen α-acetonitrile.

2.4. Qualitative Molecular Orbital Description of $\{CH_3CN\}_2^-$. Having established the nature of the dimer radical anion in the previous section, it is remarkable how the main features of the spin distribution and of the $^2B_u \leftarrow {}^2A_g$ electronic transition can be accounted for by simple MO considerations. Figure 7 shows a correlation diagram that indicates how the in-plane π and π* orbitals of the two initially linear acetonitrile molecules interact on coming together in an antiparallel arrangement along a C−C symmetry axis connecting the cyanide carbons. As shown, the transformation of the two π and two π* orbitals into the σ orbitals of the transoid dimer is accompanied by the outward bending of the CCN fragments as the latter approach each other along this C−*C* axis. Of particular interest is the fact that the $\pi_1 - \pi_2$ and $\pi_1{}^* + \pi_2{}^*$ combinations associated with the intermediate energy levels correspond quite closely to the generation of the frontier orbitals no. 22 and no. 23, these consisting of the doubly occupied subjacent b_u MO and of the a_g singly occupied molecular orbital (SOMO), respectively, shown in Figures 5a and 5b.

In the simplest representation, therefore, these orbitals may be said to resemble the two allowed $\pi_1 - \pi_2$ and $\pi_1{}^* + \pi_2{}^*$ combinations, these being formed primarily from the *nonbonding* in-plane N 2*p* orbitals, although there are smaller but significant coefficients on the carbon atomic orbitals directed mainly along the $C-CH_3$ bonds. On the basis of this simple model, it is immediately understandable why the spin distribution characteristic of the a_g SOMO is so heavily weighted in favor of the nitrogen atoms, as shown by experiment and confirmed by the calculations. Moreover, because of the dominant nitrogen contribution, the bending at the cyanide carbon does not introduce appreciable spin density into the corresponding C 2*s* orbital, in sharp contrast to the spin distribution found for the CH_3CN^- monomer radical anion (see below). Thus, the bonding between the cyanide carbons in the dimer radical anion (which would be largely attributable to the filled $\pi_1 + \pi_2$ combination in the simple MO model) has the effect of localizing the spin on nitrogen. This in turn means that the cyanide ^{13}C hfc is not a reliable measure of the extent to which the acetonitrile molecules are bent from linearity in the dimer, contrary to earlier considerations.[19]

It is also noteworthy that the simple MO diagram predicts that the a_g SOMO is bonding between the cyanide carbons but is C−N antibonding, whereas the reverse situations apply for the b_u subjacent orbital No. 22. Thus, the shorter NC−CN distance calculated for the ^2B_u excited state is consistent with electron promotion from the filled b_u to the a_g orbital. Moreover, the calculation also yields smaller CCN angles and longer $C-CH_3$ bonds for the ^2B_u excited state as compared to the ^2A_g state, which is indicative of the increased C−N antibonding interaction resulting from the filled a_g orbital.

3. Monomer Radical Anion in *β*-Acetonitrile

The crystal structure of *β*-CD_3CN is shown in Figure 2.[32] This crystal consists of several infinite chains of “parallel” acetonitrile molecules; there are no “antiparallel” pairs as in α-acetonitrile. The molecules are symmetric with respect to the (100) plane; their C and N atoms lying in this plane (Figure 2). Two $\{CD_3CN\}_\infty$ chains with a period of 3.5 Å point in the direction of the (110) vector and occupy $(3\bar{3}\bar{5})$ and $(\bar{3}3\bar{5})$ planes, respectively. These two chains are symmetric with respect to their planes and are transformed into each other by a C-glide reflection in the (010) plane. The shortest approach between the neighboring molecules is within the short-period chains (shown separately in Figure 5S). Two other chains, with a period of $a = 5.99$ Å, point in the direction of axis **a** (Figure 2); the C and N atoms of these chains occupy the (0, ±345, −580) planes. These chains are transformed to each other by a **c** glide reflection in the (010) plane.

EPR parameters for two variants, site-1 and site-2, of monomer anions in *β*-acetonitrile and high-temperature adiponitrile-*d*$_8$ are given in Table 2 (after ref 30); the directional cosines are given in Table 4S (see the stereographic projection in Figure 21S). In adiponitrile-*d*$_8$, the long axes of g- and ^{14}N hfc tensors for both sites are coaxial within 3°. In *β*-acetonitrile, the long axes of g-, ^{14}N and ^{13}CN hfc tensors are coincident within 10° and point in the same direction for both sites (Table 4S and Figure 21S). The g- and ^{13}CN hfc tensors are coaxial within 13°. The **b** axes of g and ^{14}N tensor make 47° in the plane perpendicular to their common **c** axis. It is not clear, whether this orientation is correct because the EPR spectra are congested and small line splittings due to axial components of the ^{14}N hfc tensor cannot be followed with certainty. The g- and ^{13}CN tensors of the two anion variants transform into each other by a 76° rotation around their common **c** axis.

Although the principal values and axes of the hfc tensor for ^{14}N given in Tables 2 and 4S may need correction, there is much similarity between the g-tensor and hfc tensors for the two nitrile anions and HCN^- (Table 2). The structures are, of course, expected to be similar. According to ref 46, HCN^- is a bent anion with the HCN angle of 131°; the spin densities for 2*p* orbitals on the cyanide C and N are 0.32 and 0.41, respectively. For CH_3CN^-, these spin densities are 0.19 and 0.55.[19] Using Coulson's formula, Williams and Sprague estimated that the CCN angle is ∼130°.[19]

As mentioned in the Introduction, in the gas phase the electron attaches to CH_3CN to produce a dipole-bound anion whose structure is very different from that of the monomer anion in

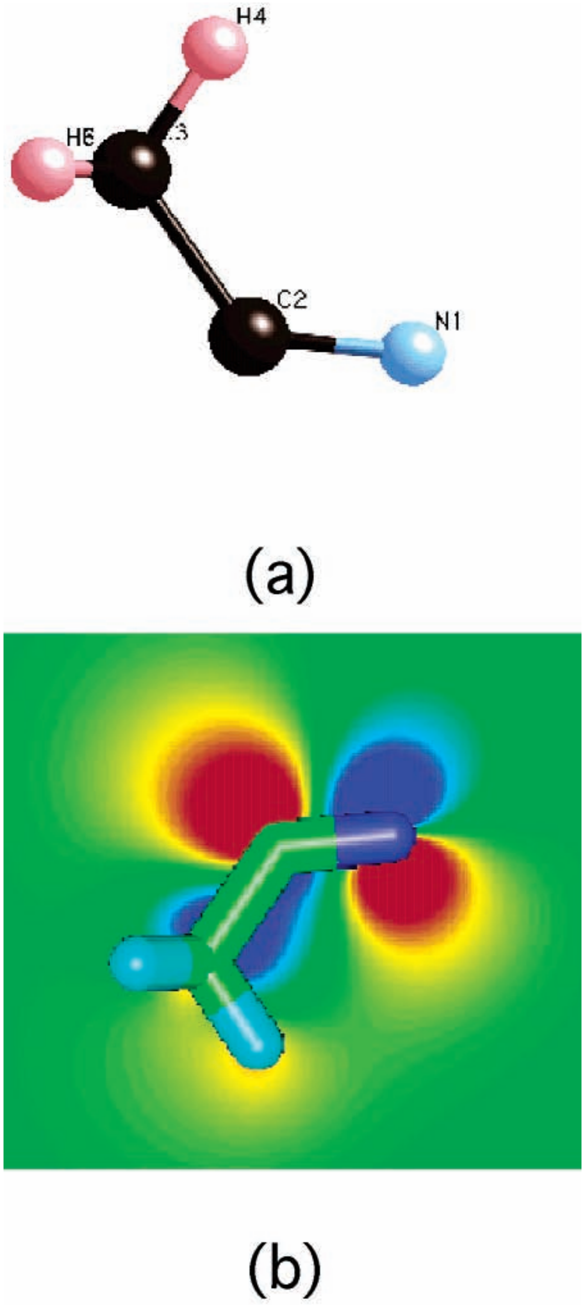

Figure 8. (a) Optimum geometry CH_3CN^- anion obtained in a DFT calculation using the B3LYP/6-31+G** IEFPCM method of Tomasi et al. (ref 43). The monomer anion has the C_s symmetry; the anion is "solvated" by liquid acetonitrile. See Table 6 for the angles and bond lengths. (b) The contour plot of the SOMO.

β-acetonitrile.[8−11] Thus, to model the structure of CH_3CN^- one needs to "force" the excess electron into valence orbitals. This may be accomplished in two different ways: (i) by using tight-binding basis sets that lack diffuse orbitals and (ii) using "solvation" models (such as IEF PCM) in which the energy of CH_3CN^- is lowered by polarization of the media. In the latter case, polarized and diffuse functions may be provided. The second method gives better results. The first method tends to produce unrealistically large isotropic hfc constants on carbons. In these DFT calculations, the C_s symmetry was imposed.

Figure 8 shows the optimum geometry and the SOMO for CH_3CN^- anion obtained using the B3LYP/6-31+G**/IEFPCM model. The orientation of in-plane principal axes of hfc tensors is shown in Figure 22S. Table 6 gives angles, bond lengths, and hfc tensors obtained in several DFT calculations. While there is a considerable spread between these parameters, all of these DFT calculations give the $^2A'$ state with the CCN angle of 125−130° as the lowest state of the monomer anion. In particular, the B3LYP/6-31+G**/IEFPCM model yields a monomer anion whose geometry is very similar to that of the CH_3CN half of the dimer anion (see above). A comparison between the calculated EPR parameters in Table 6 and those given in Table 2 shows that the DFT calculations give reasonable estimates for the isotropic hfc constants for both carbons and provide close estimates for the isotropic hfc constant for ^{14}N. However, these calculations give hfc tensors that are considerably more axial in character than those observed for CD_3CN^- in β-acetonitrile. This suggests that the monomer anion does not retain the planar symmetry of the $\{CD_3CN\}_\infty$ chains.

Using CIS/6-31G, we estimate that a vertical transition from the ground $^2A'$ state to the first excited state ($^2A''$) occurs at 2.4−2.8 eV (Table 6). In the experimental spectra, the absorption band peaks at 2.95 eV. No bound-to-bound IR transitions for the monomer anion were obtained. Thus, both the DFT calculation and the absorption data for CH_3CN^- in β-acetonitrile suggest that the IR absorbing anion-1 in liquid acetonitrile cannot be the monomer radical anion.

The orientation of the CD_3CN^- anion in β-acetonitrile may be guessed from the data of Tables 2 and 4S. In a *Cmc*2$_1$ crystal, the sites are transformed to each other by (i) reflection in the (100) plane and (ii) **c** glide reflection in the (010) plane. Unless the direction of the N 2*p* orbital is coincident with one of crystallographic axes, there are either two or four variants of the anion in which these 2*p* orbitals point in different directions.

TABLE 6: Optimized Geometry, EPR Parameters, and Optical Transitions for the Ground $^2A'$ State of CH_3CN^- (the C_s Symmetry)

parameter[a]	B3LYP	B3LYP	B3LYP IEF PCM	B3LYP	B3LYP IEF PCM
basis set	3-21G	6-31G	6-31G	EPR-II	6-31+G**
C2−N1	1.237	1.247	1.249	1.214	1.221
C2−C3	1.626	1.573	1.555	1.549	1.529
C3−H4	1.112	1.116	1.11	1.11	1.107
C3−H5	1.103	1.104	1.101	1.096	1.096
∠C3−C2−N1	124.7	125.3	126.3	131.9	130.5
∠C2−C3−H4	114.1	114.1	113.4	110.7	111.7
∠C2−C3−H5	109.5	110.3	110.4	109.7	110.2
∠H5−C3−C2−N1	121.6	121.4	121.4	121	121.2
$^{14}N[1]$, iso	6.99	9.2	9.22	7.7	9.33
aa	−7.3	−7.7	−7.7	−5	−6.1 (z)
bb (z)	−7.2	−7.6	−7.6	−4.9	−6
cc	14.5	15.3	15.3	9.9	12.2
$^{13}C[3]H_3$, iso	118.5	131	103.6	159.5	97.5
aa	−4.4	−4	−8.4	−2	−3
bb (z)	−3.7	−3	−7.8	−1	−2.4
cc	8.1	7	16.2	3	5.4
$^{13}C[2]N$, iso	111.4	111.7	102.3	44.8	46.9
aa (z)	−7.4	−7.5	−8.4	−5.2	−6.5
bb	−6.5	−7.5	−7.8	−5.2	−5.5
cc	13.9	15	16.2	10.4	12
∠**c**(N),**c**(CN)	40.7	35.6	29.7	33.4	28.3
∠**c**(N),**c**(CH_3)	59.3	60.2	58.1	63.4	56.5
excited state		$^2A''$	$^2A''$	$^2A'$	
energy vs $^2A'$		2.74	2.66	2.39 *(2.95)*	
f		0.0026	0.0026	0.089 *(0.072)*	
ΔG_{solv}[b]			−2.5		−2.33

All calculations are done using DFT methods in Gaussian 98 package (ref 37). [a] The bond lengths are given in Å, the angles in degrees, energies in eV; hfc constants in Gauss; the z axis is normal to the symmetry plane. [b] IEF PCM method of Tomasi et al. (ref 43).

Experimentally, the directions of the C and N 2*p* orbitals (long axes of g-, ^{13}CN, and ^{14}N tensors) are the same for both sites. According to DFT calculations, these 2*p* orbitals lie in the CCN plane of the anion (Figures 8 and 22S), and rotation of the methyl group has little effect on this orbital alignment. If these 2*p* orbitals were in the direction of axes **b** or **c** of the crystal, the CCN fragment of the anion would be in the (100) plane. In such a case, only one variant of the anion would be observed by EPR. Therefore, the only possible orientation of these 2*p* orbitals (the *y* axis of the laboratory frame, Figure 21S) is in the direction of crystallographic axis **a**. This axis is also the direction of $\{CD_3CN\}_\infty$ chains shown in Figure 2. We suggest that the CCN fragment of the anion retains the $(0,345,-580)$ and $(0,-345,-580)$ planes of these two chains; consequently, there are two variants of the anion. The angle between these two planes is 83°, which is reasonably close to 76° obtained for the angle between the **c**[g] axes for site-1 and site-2 (see above). To observe two (rather than four) variants of the CD_3CN^- and $CD_3{}^{13}CN^-$ anion, the cyanide group has to reside in the same (100) plane as that of the neutral molecule. For $^{13}CD_3C^{14}N$, there should be four variants differing in the orientation of the $^{13}CD_3$ hfc tensor. However, this tensor is spherically symmetrical (Table 2), and the two additional variants are not spectrally distinguishable.

The methyl groups of acetonitrile molecules in the long-period chain are not symmetric with respect to the $(0,\pm345,-580)$ plane; actually, the CCH plane is normal to this plane (which we identify with the CCN plane). This lack of C_s symmetry may account for the nonaxiality of the hfc tensors.

4. Conclusions

Using EPR, optical spectroscopy, and *ab initio* calculations, we demonstrate that electron attachment to nitrile molecules causes bending of their CCN fragments to ca. 130°. In the resulting radical anions, the NC−C bond is 6−8% longer than in the parent molecules, which accounts for the ease of C−C fragmentation of the radical anion upon photoexcitation.

The dimer anion exhibits C_{2h} symmetry. In its ground ^2A_g state, there is a pseudo bond (1.65−1.7 Å) between the cyanide carbons; all properties of the dimer anion depend on the strength of this bond. The staggered structures shown in Figure 4 account for the observed EPR parameters (Table 1), the position of the $^2B_u \leftarrow {}^2A_g$ absorption band, and the vibronic progressions in the latter. A further confirmation of this structure might become possible using matrix isolation IR spectroscopy (see, for example, ref 47).

In α-acetonitrile, which consists of stacks of antiparallel $\{CH_3CN\}_2$ pairs, the dimer radical anion retains the same crystallographic plane as these pairs. These dimer radical anions form only in crystals where such "antiparallel" pairs occur; otherwise, the electron localizes on a single molecule, as in *β*-acetonitrile. In the latter crystal, the monomer anion seems to retain the crystallographic plane of the $\{CH_3CN\}_8$ chain. In both of these crystals, the radical anions are stabilized by the surrounding molecules: no such structures can exist in the gas phase.

According to NMR and X-ray diffraction studies,[48] the structure of liquid acetonitrile is similar to that of crystalline α-acetonitrile, with a pentamer as a basic unit. In this pentamer, there are two "antiparallel" pairs similar to those observed in α-acetonitrile. Such a structure naturally accounts for the formation of anion-2 whose absorption band and photochemical properties are similar to those of the dimer radical anion in frozen α-acetonitrile. It also explains why the formation of a stable monomer radical anion in the liquid is unlikely: such an anion would immediately couple to a neighboring "antiparallel" molecule. This propensity for C−C bond formation, once the negative charge is shared by the solvent molecule(s), is what distinguishes acetonitrile from water and alcohols. Another factor is the large dipole moment that, due to a lack of hydrogen bonding, leads to close antiparallel pairing of neighboring solvent molecules; this pairing greatly facilitates the formation of the dimer anion. As argued in ref 18, the "solvated electron" can still occur in liquid acetonitrile, but now this is no longer the lowest energy state of the excess electron.

Acknowledgment. I.A.S. thanks Dr. U. Geiser for his help with crystallographic analyses. This work was performed under the auspices of the Office of Science, Division of Chemical Science, US-DOE under contract No. W-31-109-ENG-38.

Supporting Information Available: (1) Captions to Figures 1s to 22S; (2) Tables 1S to 4S; (3) a PDF file containing Figures 1S to 22S; (4) a PDF file containing color Figures 1 to 8. This material is available free of charge via the Internet at http://pubs.acs.org.

References and Notes

(1) *Excess Electrons in Dielectric Media*; Ferradini, C., Jay-Gerin, J.-P., Eds.; CRC Press: Ann Arbor, 1991; Pikaev, A. K. *Solvated Electron in Radiation Chemistry*; Israel Program for Scientific Translations, Jerusalem, 1971.

(2) Kevan, L. *J. Phys. Chem.* **1978**, *82*, 1144.

(3) Springlet, B. E.; Jortner, J.; Cohen, M. H. *J. Chem. Phys.* **1968**, *48*, 2720; Jortner, J. *Ber. Bunsen-Ges. Phys. Chem.* **1971**, *75*, 696.

(4) Brodsky, A. M.; Tsarevsky, A. V. *Adv. Chem. Phys.* **1980**, *44*, 483; *J. Phys. Chem.* **1984**, *88*, 3790.

(5) Sheu, W.-S.; Rossky, P. J. *J. Am. Chem. Soc.* **1993**, *115*, 7729.

(6) Borgis, D.; Staib, A. *J. Chem. Phys.* **1996**, *104*, 9027.

(7) Motakabbir, K. A.; Schnitker, J.; Rossky, P. J. *J. Chem. Phys.* **1992**, *97*, 2055.

(8) Illenberger, E. *Chem. Rev.* **1992**, *92*, 1589; Abdoul-Carime, H.; Bouteiller, Y.; Desfrançois, C.; Philippe, L.; Schermann, J. P. *Acta Chem. Scand.* **1997**, *51*, 145; Desfrançois, C.; Abdoul-Carmie, H.; Adjouri, C.; Khelifa, N.; Schermann J. P *Europhys. Lett.* **1994**, *26*, 25; Stockdale, J. A.; Davis, F. J.; Compton, R. N.; Klots, C. E. *J. Chem. Phys.* **1974**, *60*, 4279; Sugiura, T.; Arakawa, A. In *Proceedings of the International Conference on Mass Spectroscopy*; University of Tokyo: Tokyo, 1970; p 848.

(9) Bailey, C. G.; Dessent, C. E. H., Johnson, M. A.; Bowen, Jr., K. H. *J. Chem. Phys.* **1996**, *104*, 6976.

(10) Popple, R. A.; Finch, C. D.; Dunning, F. B. *Chem. Phys. Lett.* **1995**, *234*, 172.

(11) Renner, T. A.; Blander, M. *J. Phys. Chem.* **1977**, *81*, 857.

(12) Siebers, J. G.; Buck, U.; Beu, T. A. *Chem. Phys.* **1998**, *129*, 549.

(13) Mitsuke, K.; Kondow, T.; Kuchitsu, K. *J. Phys. Chem.* **1986**, *90*, 1505.

(14) Desfrançois, C., et al. *Z. Phys. D* **1992**, *24*, 297; Desfrançois, C., et al. *J. Chem. Phys.* **1991**, *95*, 7760; Bowen, K., et al. *J. Chem. Phys.* **1990**, *92*, 3980; Bowen, K., et al. *Z. Phys. D* **1991**, *20*, 9; Barnett, R. N., Landman, U.; Cleveland, C. L.; Jortner, J. *Phys. Rev. Lett.* **1987**, *59*, 811; Barnett, R. N., Landman, U.; Cleveland, C. L.; Jortner, J. *J. Chem. Phys.* **1988**, *88*, 4429; Kim, K. S.; Park, I.; Lee, S.; Cho, K.; Lee, J. Y.; Kim, J.; Joannopoulos, J. D. *Phys. Rev. Lett.* **1996**, *76*, 956 and references therein; Turi, L. *J. Chem. Phys.* **1999**, *110*, 10 364.

(15) Bell, I. P.; Rodgers, M. A. J.; Burrows, H. D. *J. Chem. Soc.* **1976**, 315.

(16) Singh, A.; Gesser, H. D.; Scott, A. R. *Chem. Phys. Lett.* **1968**, *2*, 271.

(17) Mulac, W. A.; Bromberg, A.; Meisel, D. *Radiat. Phys. Chem.* **1985**, *26*, 205.

(18) Shkrob, I. A.; Sauer, M. C., Jr. *J. Phys. Chem. A* **2002**, *106*, 9120.

(19) Williams, F.; Sprague, E. D. *Acc. Chem. Res.* **1982**, *15*, 408; Bonin, M. A.; Chung, Y. J.; Sprague, E. D.; Takeda, K.; Wang, J. T.; Williams, F. *Nobel Symp.* **1972**, *22*, 103. The photodissociation and subsequent thermal recovery of the dimer and monomer radical anions in α- and *β*-acetonitrile, respectively, has been studied extensively. See Le Roy, R. J.; Sprague, E. D.; Williams, F. *J. Phys. Chem.* **1972**, *76*, 546 and Le Roy, R. J.; Murai, H.; Williams, F. *J. Am. Chem. Soc.* **1980**, *102*, 2325 on the role of quantum-

mechanical tunneling in the H-atom abstraction reaction by methyl radicals that competes with the recovery reaction.

(20) Ayscough, P. B.; Collins, R. G.; Kemp, T. J. *J. Phys. Chem.* **1966**, *70*, 2220; Sprague, E. D.; Williams, F. *J. Chem. Phys.* **1971**, *54*, 5425.

(21) Bonin, M. A.; Takeda, K.; Tsuji, K.; Williams, F. *Chem. Phys. Lett.* **1968**, *2*, 363.

(22) Bonin, M. A.; Takeda, K.; Williams, F. *J. Chem. Phys.* **1969**, *50*, 5423.

(23) Egland, R. J.; Symons, M. C. R. *J. Chem. Soc. A* **1970**, 1326; Chandra, H.; Symons, M. C. R. *J. Chem. Soc., Faraday Trans. 1* **1988**, *84*, 3401.

(24) Holloman, L.; Sprague, E. D.; Williams, F. *J. Am. Chem. Soc.* **1970**, *92*, 429.

(25) Campion, A.; Williams, F. *J. Chem. Phys.* **1971**, *54*, 4510.

(26) Campion, A.; Ghormley, J. A.; Williams, F. *J. Am. Chem. Soc.* **1972**, *94*, 6302.

(27) Sargent, F. P., Bailey, M. G.; Gardy, E. M. *Can. J. Chem.* **1974**, *52*, 2171; Sprague, E. D.; Takeda, K.; Wang, J. T.; Williams, F. *Can. J. Chem.* **1974**, *52*, 2840.

(28) Gillbro, T.; Takeda, K.; Williams, F. *J. Chem. Soc., Faraday Trans. 2* **1974**, *70*, 465.

(29) Sprague, E. Ph.D. Thesis, University of Tennessee, Knoxville, TN, June 1971.

(30) Takeda, K. Doctor Thesis, Kyoto University, Kyoto, Japan, 1972.

(31) Barrow, M. J. *Acta Crystallogr. B* **1981**, *37*, 2239.

(32) Torrie, B. H.; Powell, B. M. *Mol. Phys.* **1992**, *75*, 613.

(33) Derollez, P.; Lefebvre, J.; Descamps, M.; Press: W.; Fontaine, H. *J. Phys. Condens. Matter* **1990**, *2*, 6893.

(34) Descamps, M. *Solid State Comm.* **1974**, *14*, 77.

(35) Fletcher, W. H.; Shoup, C. S. *J. Mol. Struct.* **1963**, *10*, 300.

(36) Knözinger, K.; Leutloff, D.; Wittenbeck, R. *J. Mol. Struct.* **1980**, *60*, 115.

(37) Frisch, M. J.; Trucks, G. W.; Schlegel, H. B.; Scuseria, G. E.; Robb, M. A.; Cheeseman, J. R.; Zakrzewski, V. G.; Montgomery, J. A., Jr.; Stratmann, R. E.; Burant, J. C.; Dapprich, S.; Millam, J. M.; Daniels, A. D.; Kudin, K. N.; Strain, M. C.; Farkas, O.; Tomasi, J.; Barone, V.; Cossi, M.; Cammi, R.; Mennucci, B.; Pomelli, C.; Adamo, C.; Clifford, S.; Ochterski, J.; Petersson, G. A.; Ayala, P. Y.; Cui, Q.; Morokuma, K.; Malick, D. K.; Rabuck, A. D.; Raghavachari, K.; Foresman, J. B.; Cioslowski, J.; Ortiz, J. V.; Stefanov, B. B.; Liu, G.; Liashenko, A.; Piskorz, P.; Komaromi, I.; Gomperts, R.; Martin, R. L.; Fox, D. J.; Keith, T.; Al-Laham, M. A.; Peng, C. Y.; Nanayakkara, A.; Gonzalez, C.; Challacombe, M.; Gill, P. M. W.; Johnson, B. G.; Chen, W.; Wong, M. W.; Andres, J. L.; Head-Gordon, M.; Replogle, E. S.; Pople, J. A. *Gaussian 98*, revision A.1; Gaussian, Inc.: Pittsburgh, PA, 1998.

(38) Møller, C.; Plesset, M. C. *Phys. Rev.* **1934**, *46*, 618; Frisch, M. J.; Head-Gordon, M.; Pople, J. A. *Chem. Phys. Lett.* **1988**, *153*, 503; Frisch, M. J.; Head-Gordon, M.; Pople, J. A. *Chem. Phys. Lett.* **1990**, *166*, 275; Frisch, M. J.; Head-Gordon, M.; Pople, J. A. *Chem. Phys. Lett.* **1990**, *166*, 281.

(39) Becke, A. D. *Phys. Rev. A* **1988**, *38*, 3098.

(40) Lee, C., Yang, W.; Parr, R. G. *Phys. Rev. B* **1988**, *37*, 785.

(41) Slater, J. C. *Quantum Theory of Molecules and Solids, v. 4: The Self-Consistent Field for Molecules and Solids*; McGraw-Hill: New York, 1974.

(42) Vosko, S. H.; Wilk, L.; Nusair, M. *Can. J. Phys.* **1980**, *58*, 1200.

(43) Tomasi, J.; Persico, M. *Chem. Rev.* **1994**, *94*, 2027; Cancès, E.; Mennucci, B.; Tomasi, J. *J. Chem. Phys.* **1997**, *107*, 3032.

(44) Barone, V. In *Recent Advances in DFT Methods, Part I*; Chong, D. P., Ed.; World Scientific: Singapore, 1996.

(45) Foresman, J. B.; Head-Gordon, M.; Pople, J. A.; Frisch, M. J. *J. Phys. Chem.* **1992**, *96*, 135.

(46) Adrian, F. J.; Cochran, E. L.; Bowers, V. A.; Weatherley, B. C. *Phys. Rev.* **1969**, *177*, 129.

(47) Zhou, M.; Andrews, L. *J. Chem. Phys.* **1999**, *110*, 2414 and 6820; Thompson, W. E.; Jacox, M. E. *J. Chem. Phys.* **1999**, *111*, 4487; Thompson, W. E.; Jacox, M. E. *J. Chem. Phys.* **1989**, *91*, 1410.

(48) Michel, H.; Lippert, E. In *Organic Liquids*; Buckingham, A. D., Lippert, E., Bratos, S., Eds.; Wiley: New York, 1978; p 293; see also p 13; Jackowski, K. *Chem. Phys. Lett.* **1992**, *194*, 167 and references therein.